ELSEVIER

Contents lists available at ScienceDirect

International Journal of Solids and Structures

journal homepage: www.elsevier.com/locate/ijsolstr





Physics and chemistry-based constitutive modeling of photo-oxidative aging in semi-crystalline polymers

Aimane Najmeddine ^a, Zhen Xu ^b, Gehui Liu ^b, Zacary L. Croft ^b, Guoliang Liu ^{b,c}, Alan R. Esker ^{b,c}, Maryam Shakiba ^{a,c,*}

- a Department of Civil and Environmental Engineering, Virginia Tech, USA
- ^b Department of Chemistry, Virginia Tech, USA
- ^c Macromolecules Innovation Institute, Virginia Tech, USA

ARTICLE INFO

Keywords: Photo-oxidation aging Semi-crystalline polymers Large deformation Polymer aging Chemi-crystallization Minute mass loss Physio-chemical characterization

ABSTRACT

This paper proposes a physio-chemically-based constitutive framework to predict the response of severely photo-oxidatively aged semi-crystalline polymers. Photo-oxidation induced by the exposure to Ultra-Violet (UV) light and oxygen is one of the main and dominant degradation mechanisms affecting the lifespan of polymers. In this work, we first characterize the physio-chemical changes of low-density polyethylene (LDPE) to understand and map the photo-oxidation degradation process. Changes in crystallinity and mass loss are characterized by Differential Scanning Calorimetry (DSC) and Quartz Crystal Microbalance with Dissipation Monitoring (OCM-D) experiments, respectively. The evolution of crystallinity and mass loss relative to the initial pristine films over exposure time are considered as indicators of material degradation. Based on these tests, we then propose evolution functions for the material properties in the polymer constitutive equations to incorporate the effects of photo-oxidation on the mechanical responses. Connecting the physio-chemical processes affecting polymer network evolution to the mechanical response of LDPE eliminates the need for defining extra fitting parameters that carry no physical meaning. The developed constitutive framework is validated with respect to a series of in-house uniaxial tensile tests performed on LDPE aged for different UV exposure times. Validation of the proposed constitutive framework confirms the accuracy of DSC and QCM-D as rigorous techniques in the characterization of degradation in LDPE films, and confirms the robustness of the developed framework in predicting the mechanical responses of photo-oxidatively aged LDPE.

1. Introduction

Over the last few decades, semi-crystalline polymers have found their way into almost all outdoor structural applications (e.g., automotive and aerospace industries, electrical insulation technologies, and thermal storage applications) due to their excellent mechanical performance and optimal strength-to-weight ratio. During their service life, semi-crystalline polymers are exposed to several extreme environmental factors such as Ultra-Violet (UV) light, heat, oxygen, and other chemical processes that degenerate their mechanical properties and contribute to their permanent failure. In particular, UV light emitted by the sun or other artificial sources in addition to the presence of oxygen has been found to be the dominant degradation mechanism causing failure and the fragmentation of semi-crystalline polymers into smaller-scaled particles known as microplastics (Rabek, 1994; Yousif and Haddad, 2013; Ranjan and Goel, 2019; Guo and Wang, 2019). Due to their minuscule sizes, microplastics can easily travel in large

amounts through water pathways leading to the ocean. The abundance of microplastics in the marine environment has become a major concern in today's environmental discussion (Kershaw and Rochman, 2015; Brandon et al., 2016; Da Costa et al., 2018; Bergmann et al., 2019). Therefore, it is imperative that special attention be devoted to the study of photo-oxidation impacts on semi-crystalline polymers for durable design and environmental preservation.

Photo-oxidation and its deleterious effects on the lifespan of semi-crystalline polymers has been a subject of experimental investigation for decades (Carrasco et al., 2001; Hsu et al., 2012; Celina, 2013; Bhateja, 1983; Fayolle et al., 2008; Julienne et al., 2019a; Hedir et al., 2020; Cundiff et al., 2020; Mohammadi et al., 2021). In general, the resistance of polymers to photo-oxidation varies depending on the polymer composition, possible inherent contaminants, and the inclusion of pigments, additives, or fillers. Polymers with weak bond energies and a high concentration of chromophores (i.e., chemical

E-mail address: mshakiba@vt.edu (M. Shakiba).

^{*} Corresponding author.

groups that are capable of absorbing light) are generally more susceptible to photo-oxidation. In semi-crystalline polyolefins, for instance, photo-oxidation can be initiated either through hydroperoxide decomposition or through ketone photolysis via Norrish reactions (Rabek, 1994). As a result of these initiators, polymers can undergo an initial period of random chain-scission followed by a secondary period of crosslinking that is responsible for surface embrittlement. Due to this embrittlement, the polymers harden and visible cracks can potentially occur on their surface (Rodriguez et al., 2020). A common consensus in the literature is that in semi-crystalline polymers, photo-oxidation reactions occur in the amorphous region that is favorable to oxygen diffusion (Ayoub et al., 2020; Rodriguez et al., 2020). The random coil structure of the amorphous region favors dynamic chain entanglements. As a result, when the polymer is exposed to light and oxygen, photooxidation-induced molecular chain alterations (i.e., chain-scission and crosslinking) manifest themselves in the unstructured, random amorphous phase. Therefore, given these considerations, it is clear that the macromolecular changes induced by photo-oxidation can be directly linked to the mechanical response (e.g., embrittlement, crack initiation and propagation, etc.) of photo-oxidatively aged polymers.

Many researchers have developed constitutive models to simulate the response of polymeric and elastomeric materials to environmental conditions (e.g., Soares et al., 2008, 2010; Vieira et al., 2014, 2011; Breche et al., 2016a,b; Wang et al., 2010; Han and Pan, 2009; Zhao and Zikry, 2017; Johlitz et al., 2014; Abdelaziz et al., 2019; Shakiba and Najmeddine, 2021; Shakiba et al., 2016). However, to the best knowledge of the authors, only a few studies tried to develop constitutive equations to study the behavior of semi-crystalline polymers in response to photo-oxidation. Belbachir et al. (2010) and Ayoub et al. (2020) used physics-based elasto-viscoplastic constitutive relationships to incorporate the effects of UV radiation on the mechanical properties of polylactic acid (PLA) and low-density-polyethylene (LDPE), respectively. More recently, Lamnii et al. (2021) captured the effect of UV radiation on the fatigue life of a bulk semi-crystalline polymer based on two indicators: the maximum true stress and the dissipated energy. These researchers used the evolution of the molecular weight of photooxidatively aged polymers to define a degradation parameter suitable for macromechanical response prediction. However, a major limitation to all these studies concerned the identification of the evolution of material properties which contained fitting parameters that carried no physical meaning. The evolution of the material properties in these studies was obtained simply by fitting the constitutive equations to the already obtained experimental mechanical measurements on aged samples. Doing so renders the constitutive equations essentially a fitting algorithm that can only describe the particular scenario upon which the calibration was performed. In contrast, purely physio-chemicallybased evolution functions of the material properties, based on network evolution, are desirable to eliminate the need for fitting parameters.

Thus, although much work has been accomplished in the experimental and the numerical sides, a robust link between the network evolution and the mechanical responses in photo-oxidative aging of polymers is still missing. Our goal is to present a physio-chemically-based constitutive framework to predict the macromechanical behavior of semi-crystalline polymers in response to photo-oxidation. We choose as material of interest LDPE due to the fact that various types of polyethylene have been found in abundunt amounts among plastic wastes in oceans and the arctic snow (Bergmann et al., 2019; Julienne et al., 2019b). We conduct chemical characterization tests to investigate the effects of photo-oxidation on the mechanical performance of LDPE and connect the resulting macromolecular changes to the evolution of material properties in the constitutive framework. It should be mentioned that more severe UV radiation compared to the previous studies is considered in this work.

This manuscript is organized as follows. Section 2 reiterates the objectives and main contributions of this work. Section 3 provides a concise description of the constitutive framework that has been

adopted in this work to describe the mechanical response of unaged LDPE. In Section 3.2, a detailed discussion on photo-oxidation processes is provided to propose a novel methodology to monitor changes in the material properties of LDPE due to photo-oxidation. Then, upon identification of the physio-chemical processes responsible for photo-oxidation of LDPE, we present in Section 4 the in-house experimental investigations proposed to determine our evolution functions for the material properties. Results and their corresponding analyses are provided in Section 5. Finally, Section 6 concludes with some important remarks and ideas for subsequent future investigations.

2. Objectives

This paper will contribute to the missing relationship between the macromolecular changes and the mechanical responses of semicrystalline LDPE due to photo-oxidation. To achieve this, a framework is developed to connect the evolution of the material properties in the constitutive equations to the physio-chemical changes in the polymer network. This connection eliminates the need to conduct mechanical testing on aged polymers and bypasses the need for extra fitting parameters. Our objectives are summarized as follows:

- First, based on our understanding of how photo-oxidation affects semi-crystalline polymers, we aim to develop a physically-based and chemically-motivated constitutive framework to predict the response of photo-oxidatively aged LDPE.
- The chemical characterization techniques employed in this work are Differential Scanning Calorimetry (DSC) and a Quartz Crystal Microbalance with Dissipation Monitoring (QCM-D). DSC and QCM-D are used to determine the evolution of the crystallinity and minute mass ratio between the initial unaged thin polymer and the corresponding aged samples, respectively.
- Second, we plan to verify the validity of employing the above characterization techniques (particularly QCM-D) on thin polymers to investigate the photo-oxidation of relatively thicker films.

Although the mass loss characterizes the direct damage from physiochemical reactions of the polymer during aging, to the best of our knowledge, there exists currently no study that uses the mass loss evolution to quantify the degree of photo-oxidation in polymers. The primary reason of the missing of mass ratio as a damage indicator is the difficulty of mass change determinations at microgram or even nanogram scale. Minute mass determination based on ordinary techniques is often unreliable due to the low sensitivity of analytical balance to mass change at micro- or nanoscale. In contrast, QCM-D, an acoustic technique, provides sensitive detection of mass change and high accuracy to nanogram-scale, which can be a solution to this challenge, thus fulfilling the deficiency of minute mass loss evolution in the literature.

3. Constitutive and governing equations

In this section, we first describe the constitutive relationships governing the mechanical response of unaged semi-crystalline polymers, and later present the framework accounting for the contribution of photo-oxidation to polymer mechanical degradation. The effect of photo-oxidation is captured by conjecturing appropriate chemistry-based evolution functions for the material properties of LDPE. Our goal is to predict the macromechanical response of photo-oxidatively aged LDPE based solely on the chemical macromolecular changes occurring in the material upon exposure to UV radiation. Note that in this work, we are only concerned with evaluating the mechanical responses of aged LDPE prior to fracture. As such, we do not include fracture in our modeling effort.

3.1. Constitutive equation of unaged semi-crystalline polymer

A number of studies in the literature have tried to develop constitutive relationships to describe the finite-strain elasto-viscoplastic behavior of polymers (Boyce et al., 1988; Arruda et al., 1995; Bardenhagen et al., 1997; Tervoort et al., 1997; Boyce et al., 2000; Ahzi et al., 2003; Anand and Gurtin, 2003; Makradi et al., 2005; Dupaix and Krishnan, 2006; Ayoub et al., 2010). The three-dimensional physicsbased constitutive theory of Boyce et al. (2000) is particularly attractive due to its simplicity and its capability of simulating various behaviors of thermoplastics based on the motion of molecular chains. The constitutive relationships of Boyce et al. (2000) were originally developed to describe deformation resistance of amorphous polymers processed above their glass transition temperature. In this work, we use Boyce et al. (2000)'s constitutive relationships which is presented in Fig. 1(a). Note that other constitutive frameworks such as the Ahzi et al. (2003)'s formulation which explicitly captures the contribution from both the crystalline as well as the amorphous domains in the intermolecular branch could also be used. However, in semi-crystalline polymers, the contribution due to crystallinity shown in Fig. 1(a) can also be captured implicitly through the elastic modulus (Abdul-Hameed et al., 2014). Moreover, as explained in Abdul-Hameed et al. (2014), this comes at the cost of having to identify double the number of unknown input parameters in the intermolecular resistance branch, which overcomplicates the approach and deviates the focus from the primary objective of this work (which is to connect the underlying micromechanical changes to the overall macromechanical response in a simple self-contained constitutive framework).

In the constitutive formulation of Boyce et al. (2000), the resistance to deformation consists schematically of two nonlinear Maxwell elements connected in parallel to one another as shown in Fig. 1(b). Branch I involves a linear elastic spring to represent molecular interactions, and a nonlinear viscous dashpot to account for the non-Newtonian flow arising from the motion of polymer segments (unlinking and sliding) as shown in Fig. 1(a). The spring stiffness in Branch I implicitly considers the contribution from both the amorphous as well as the crystalline phases illustrated in Fig. 1(a). Branch N is composed of a nonlinear elastic spring (i.e., Langevin spring) representing the rubbery behavior of the polymer network based on the non-Gaussian statistical mechanics theory of rubber elasticity (Arruda and Boyce, 1993). The nonlinear spring is intended to capture the post-yield strain hardening at large strains due to the alignment of the long-chain polymer molecules. A nonlinear dashpot that is connected in series to it is included to represent the rate- and temperature-dependent flow arising from the motion of polymer segments at large strains. The inclusion of the two nonlinear dashpots captures the rate-dependency of the stress-strain behavior through molecular orientation and relaxation.

Since the branches of the schematic representation shown in Fig. 1(b) are parallel, the total deformation gradient F is applied to both branches and we have:

$$\mathbf{F} = \mathbf{F}_I = \mathbf{F}_N \tag{1}$$

where the indices I and N refer to the intermolecular and network resistance branches, respectively. The total Cauchy stress tensor T can therefore be written as the sum of the two contributions T_I and T_N :

$$\mathbf{T} = \mathbf{T}_I + \mathbf{T}_N \tag{2}$$

Next, we present details on the kinematic configuration as well as the developed constitutive framework considering photo-oxidation effects.

3.1.1. Kinematics

Both branches involve springs that are attached in series to dashpots. Therefore, the deformation gradients corresponding to each branch can be decomposed multiplicatively into elastic and plastic components as follows (Lee. 1969):

$$\mathbf{F}_{I} = \mathbf{F}_{I}^{e} \mathbf{F}_{I}^{p}$$
 and $\mathbf{F}_{N} = \mathbf{F}_{N}^{e} \mathbf{F}_{N}^{p}$ (3)

where the superscripts e and p refer to the elastic and plastic parts, respectively.

The plastic deformation gradients \mathbf{F}_I^p and \mathbf{F}_N^p can be obtained as follows:

$$\dot{\mathbf{F}}_{I}^{p} = \mathbf{F}_{I}^{e-1} \mathbf{D}_{I}^{p} \mathbf{F}_{I}^{e} \mathbf{F}_{I}^{p} \quad \text{and} \quad \dot{\mathbf{F}}_{N}^{p} = \mathbf{F}_{N}^{e-1} \mathbf{D}_{N}^{p} \mathbf{F}_{N}^{e} \mathbf{F}_{N}^{p}$$

$$\tag{4}$$

in which the rates of inelastic deformation \mathbf{D}_I^p and \mathbf{D}_N^p must be described. The dot expression denotes the time derivative $\frac{\partial}{\partial t}(\cdot)$. The elastic deformation gradients \mathbf{F}_I^e and \mathbf{F}_N^e are obtained using Eqs. (3). The derivations leading to Eqs. (4) are provided in Appendix.

3.1.2. Intermolecular branch

In this section, we explain the governing visco-elastoplastic equations corresponding to the intermolecular resistance branch. The intermolecular resistance is represented by a linear spring in series with a nonlinear dashpot. The intermolecular Cauchy stress \mathbf{T}_I is expressed in terms of the Hencky strain $\ln(\mathbf{V}_i^c)$ as:

$$\mathbf{T}_I = \frac{1}{J_i^e} C_I^e \ln(\mathbf{V}_I^e) \tag{5}$$

where $J_I^e = \det \mathbf{F}_I^e$ and \mathbf{C}_I^e is the isotropic fourth-order elastic stiffness tensor expressed as:

$$\mathbf{C}_{I}^{e} = \left(\frac{E_{0}}{1+\nu}\right) \mathbb{I} + \left(\frac{E_{0}\nu}{(\nu+1)(2\nu-1)}\right) \mathbf{I} \otimes \mathbf{I}$$
 (6)

where E_0 is the Young's modulus, ν is the Poisson's ratio, and \mathbb{I} and \mathcal{I} are the fourth- and second-order identity tensors, respectively. The symbol \otimes denotes the tensor product operation.

The viscoplastic strain rate tensor \mathbf{D}_{I}^{p} is expressed by the following flow rule:

$$\mathbf{D}_{I}^{p} = \dot{\gamma}_{I}^{p} \frac{\mathbf{DEV}(\mathbf{T}_{I})}{\sqrt{2}\tau_{I}} \tag{7}$$

where $\mathbf{DEV}(\mathbf{T}_I) = \mathbf{T}_I - \frac{tr(\mathbf{T}_I)}{3} \mathbf{I}$ is the deviatoric part of \mathbf{T}_I , $\tau_I = \frac{1}{\sqrt{2}} \| \mathbf{DEV}(\mathbf{T}_I) \|$ is the effective shear stress written in terms of the Frobenius norm $\| \mathbf{DEV}(\mathbf{T}_I) \|$ of the deviatoric part of \mathbf{T}_I , and $\dot{\gamma}_I^P$ is the viscoplastic shear strain rate given by the following expression:

$$\dot{\gamma}_I^p = \dot{\gamma}_0 exp \left[-\frac{\Delta G_{a_0}}{K_R \Theta} \left(1 - \frac{\tau_I}{s_0} \right) \right] \tag{8}$$

where $\dot{\gamma}_0$, K_B , and Θ are the pre-exponential shear strain rate factor, the Boltzmann constant, and the absolute temperature, respectively. The variables ΔG_{a_0} and s_0 are the activation energy and the athermal shear yield strength, respectively. The former is the free energy change representing the barrier to molecular mobility that must be overcome in order for plastic flow to occur while the latter represents the limit of the effective shear stress τ_I as the temperature approaches absolute zero (Boyce et al., 1988).

3.1.3. Molecular network branch

In this section, we explain the governing visco-hyper-elastoplastic equations corresponding to the molecular network resistance branch N. The molecular network resistance is represented by a nonlinear spring in series with a nonlinear dashpot. The molecular network part of the Cauchy stress \mathbf{T}_N is expressed as a function of the elastic deformation gradient \mathbf{F}_N^e using a non-Gaussian statistical framework involving the inverse of the Langevin function \mathcal{L}^{-1} (Arruda and Boyce, 1993):

$$\mathbf{T}_{N} = \frac{1}{J_{N}^{e}} \mu_{0} \frac{\sqrt{N_{k_{0}}}}{\bar{\lambda}_{N}^{e}} \mathcal{L}^{-1} \left(\frac{\bar{\lambda}_{N}^{e}}{\sqrt{N_{k_{0}}}} \right) \left[\bar{\mathbf{B}}_{N}^{e} - (\bar{\lambda}_{N}^{e})^{2} \mathbf{I} \right]$$

$$(9)$$

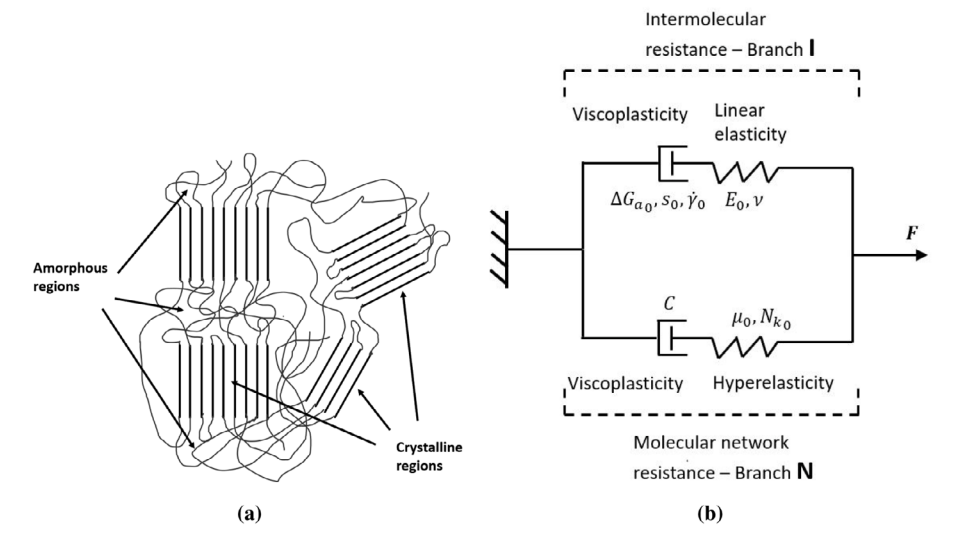


Fig. 1. (a) Schematic representation of a semi-crystalline polymer consisting of two contributing regions: an amorphous region characterized by the coil-like random arrangement, and a crystalline region characterized by the structured, orderly geometric alignment. (b) Rheological representation of the constitutive theory of Boyce et al. (2000) highlighting the contribution from the intermolecular resistance (i.e., branch I) and molecular network resistance (i.e., branch N). The elasto-viscoplastic parameters are shown attached to each corresponding element. The effects of both the amorphous as well as the crystalline regions on the mechanical resistance to deformation is captured implicitly via the elastic modulus E_0 . The total deformation gradient \mathbf{F} is applied to both branches.

where $\mu_0=nK_B\Theta$ is the rubber modulus given as a function of n the number of chains per unit volume, N_{k_0} is the number of Kuhn monomers per chain, $\mathcal{L}(\cdot)=\coth(\cdot)-\frac{1}{(\cdot)}$ is the Langevin function whose inverse is given by $\mathcal{L}^{-1}(x)=x\left(\frac{3-x^2}{1-x^2}\right)$ (Cohen, 1991), and $\bar{\lambda}_N^e=\sqrt{\frac{I_1}{3}}$ is the effective macro-stretch written as a function of the first invariant $\bar{I}_1=tr(\bar{\mathbf{B}}_N^e)$ of the elastic isochoric left Cauchy–Green deformation tensor $\bar{\mathbf{B}}_N^e=(J_N^e)^{-2/3}\mathbf{F}_N^e\mathbf{F}_N^eT$.

The flow strain rate tensor \mathbf{D}_N^p is expressed by the following flow rule:

$$\mathbf{D}_{N}^{p} = \dot{\gamma}_{N}^{p} \left(\frac{\mathbf{DEV}(\mathbf{T}_{N})}{\sqrt{2}\tau_{N}} \right) \tag{10}$$

where $\mathbf{DEV}(\mathbf{T}_N) = \mathbf{T}_N - \frac{tr(\mathbf{T}_N)}{3} \mathbf{\mathcal{I}}$ is the deviatoric part of \mathbf{T}_N , $\tau_N = \frac{1}{\sqrt{2}} \|\mathbf{DEV}(\mathbf{T}_N)\|$ is the effective shear stress, and $\dot{\gamma}_N^p$ is the flow shear strain rate given by the following expression:

$$\dot{\gamma}_N^p = C\left(\frac{\tau_N}{\lambda_N^p - 1}\right) \tag{11}$$

in which the parameter C is included to account for temperature-dependency of relaxation and $\lambda_N^p = [tr(\mathbf{B}_N^p)/3]^{1/2}$, where $\mathbf{B}_N^p = \mathbf{F}_N^p \mathbf{F}_N^p T^N$. Note that Eq. (11) is unstable for $\lambda_N^p = 1$; therefore, to ensure numerical stability, a perturbation coefficient equal to 10^{-6} is added to λ_N^p in all of our simulations.

3.2. Photo-oxidation contribution

Photo-oxidation induces alterations to the mechanical properties of semi-crystalline polymers. Upon exposure to UV light, semi-crystalline polymers undergo an initial period of chain-scission in which long molecular chains in the amorphous phase break causing a decrease in the average molar mass. As a result, segments of entangled chains in the amorphous region are released, and with enough mobility, free segments can rearrange into a crystalline region (Rabello and White, 1997). With increased crystallinity, the inter-lamellar spacing decreases and embrittlement takes place (Fayolle et al., 2008). This process is known as chemi-crystallization and is illustrated schematically in Fig. 2. During photo-oxidation, thickness of the primary crystalline region remains unchanged ($I_0^c \approx I_{aged}^{c1}$); however, thickness of the amorphous domain decreases ($I_{aged}^a < I_0^a$) and free segments begin to re-crystallize

within a newly formed crystalline domain of thickness I_{aged}^{c2} (Rodriguez et al., 2020). In other words, the amorphous region shrinks at the expense of the crystalline phase that gains further structuring ($I_0^c < I_{aged}^{c1} + I_{aged}^{c2}$). Note that we keep the distinction between primary and secondary crystallites out of discussion since such distinction is irrelevant from the perspective of the behavior of the material where crystallinity is expected to increase regardless of which label is most appropriate.

On the one hand, chemi-crystallization is indicative of a stiffening and a strengthening behavior probing intermolecular interactions. In fact, increase in crystallinity (and consequent shrinkage of the amorphous domain) as shown in Fig. 2 suggests that an increased stiffness is expected. On the other hand, chemi-crystallization also indicates an increase in the flow stress required to overcome intermolecular barriers to deformation. Therefore, it is expected that the material properties involved in the intermolecular resistance branch to change in response to photo-oxidation. In this section, we aim to arrive at appropriate evolution functions for the material properties corresponding to the intermolecular resistance branch, *i.e.*, the initial stiffness E_0 , the athermal shear yield strength s_0 , and the activation energy ΔG_{a_0} , based on the chemical understanding presented heretofore.

Remark. Recall that the material parameters involved in the constitutive relationships of Boyce et al. (2000) are: for the intermolecular resistance branch, the elastic modulus E_0 , the Poisson's ratio ν , the athermal shear yield strength s_0 , the activation energy ΔG_{a_0} , and the pre-exponential shear strain rate factor $\dot{\gamma}_0$, whereas for the network resistance branch, the rubber modulus μ_0 , the number of Kuhn monomers per chain N_{k_0} , and the constant accounting for temperaturedependency of relaxation C. The parameters ν , $\dot{\gamma}_0$, and C are assumed constant in this work. The reason for this assumption is provided as follows. Since LDPE films are tested above their glass transition temperature, we assign the value 0.49 to the Poisson's ratio ν . Additionally, at room temperature - which is where accelerated photo-oxidation aging is performed in this study – the temperature-dependent relaxation parameter C is assigned the value $8 \times 10^{-8} \text{ MPa}^{-1}$ (Boyce et al., 2000). Finally, the pre-exponential shear strain rate factor $\dot{\gamma}_0$ is assigned the value 1.75×10^6 s⁻¹ (Boyce et al., 2000). On the other hand, the rubber modulus μ_0 and the number of monomers per chain N_{k_0} are assumed to have minor effects on the response of LDPE to photo-oxidation, especially at long aging times. In fact, as the material becomes highly crystalline, it also becomes brittle and fracture occurs prematurely when mechanical load is applied (i.e., at lower strain levels). The

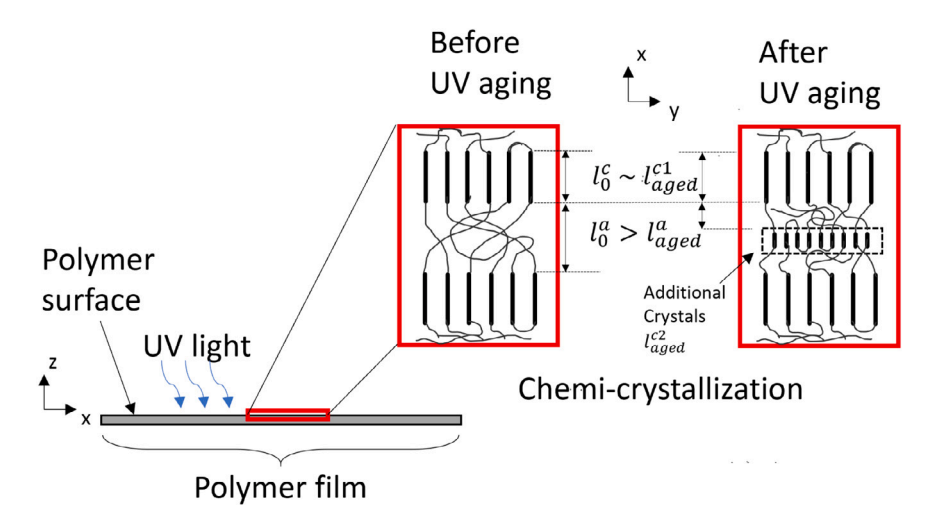


Fig. 2. Schematic representation of chemi-crystallization due to photo-oxidation. Upon exposure to UV light, the molecular chains in the amorphous region break and degrade causing the formation of additional crystals within the amorphous domain. Thickness of the primary crystalline region remains unchanged but the thickness of the amorphous domain decreases, thus allowing free segments to re-crystallize within a newly formed crystalline domain. In other words, the amorphous region shrinks ($l_{aged}^a < l_0^a$) on the expense of the crystalline phase that gains further structuring ($l_{aged}^c < l_{aeed}^c + l_{aeed}^c +$

increase in crystallinity and subsequently the premature fracture of LDPE at long aging times means that the resistance to deformation at long aging times can be captured simply by the intermolecular branch responsible for the elasto-plastic behavior. Therefore, from a mathematical standpoint, the material properties corresponding to the network resistance branch (i.e., the rubber modulus μ_0 and the number of Kuhn monomers per chain N_{k_0}) – which govern the large-strain deformation behavior, are no longer necessary. Instead, at long exposure times, the material is highly brittle and the mechanical response can be captured elasto-plastically (i.e., using only the intermolecular branch contribution).

In order to conjecture appropriate chemistry-based evolution expressions for the material properties, we first recognize that photooxidation effects are mostly surface effects (Suresh et al., 2011; Shlyapintokh, 1983; Yousif and Haddad, 2013). Photo-oxidation causes carbonyl groups to form on the surface of polyethylene and increases hydrophilicity (Suresh et al., 2011), which then leads to embrittlement. Indeed, oxidative UV aging of LDPE causes an increase in the wettability of LDPE films due to the introduction of oxygen-containing polar functional groups (hydroxyl, carbonyl, and acids) (Suresh et al., 2011). As a result, photo-oxidation-induced damage concentrates on the surface of the material. Taking these considerations into account, we propose to employ the minute mass ratio, which is a surface-sensitive technique, as the characteristic degradation indicator to photo-oxidation in LDPE. Additionally, as mentioned in the earlier discussion, changes in the molecular-surface interactions as well as the crystallinity probe the evolution of the initial stiffness in response to photo-oxidation. Therefore, we posit that the evolution of the Young's modulus where the material is degraded be expressed as follows:

$$E(t) = E_0 \left(\frac{\zeta(t)}{\zeta_0}\right) \omega(t)^{-1}$$
(12)

where E_0 and E(t) are the Young's modulii corresponding to the unaged and aged (for some time t) states, respectively, ζ_0 and $\zeta(t)$ are the crystallinities at the unaged and aged states, respectively, and $\omega(t)$ is the degradation indicator defined as minute mass ratio between the current and initial aging states (i.e., $\omega(t) = m(t)/m(0)$ where m(0) and m(t) are the polymer masses at UV exposure duration of 0 and t, respectively).

Eq. (12) captures two principles. First, the initial stiffness depends on the evolution of the crystallinity. In fact, not only does this dependence capture the increase in the initial modulus, but even situations for which the initial stiffness decreases or remains constant can be well captured. Indeed, the crystallinity can follow any type of evolution

depending on the chemical mechanism at hand. The stiffness will then follow a similar evolution (with mass loss held fixed) due to the linear proportionality of Eq. (12). Second, the effect of mass degeneration on the stiffness is taken into account through an inverse proportionality. This inverse dependence can be justified as follows. First, as previously mentioned in the manuscript, photo-oxidation effects occur predominantly in the amorphous region of semi-crystalline polymers. Therefore, any changes in the polymer's mass would suggest that the amorphous phase is perturbed on the expense of the crystalline region (see Fig. 2). Additionally, one could appreciate the parallelism between Eq. (12) and the relationship for elastomers relating the crosslink density ρ and the molar mass between two crosslinks M_c through $\rho \propto 1/M_c$. Since the stiffness is directly proportional to the crosslink density in elastomers, it must therefore be inversely proportional to the molar mass between two crosslinks. Eq. (12) captures an analogous inverse proportionally between the minute mass ratio and the stiffness, therefore adding more validity to its functionality.

In Eq. (12), aside from E_0 which can be obtained directly from a mechanical tensile test on an unaged sample, the evolution of the Young's modulus is given entirely as a function of variables that can be experimentally determined through appropriate chemical characterization tests — in this case, DSC to obtain the crystallinity ζ and the surface-sensitive technique QCM-D to obtain the degradation parameter ω . Therefore, no additional fitting variables are required, making Eq. (12) purely physio-chemically motivated. Therefore, in defining Eq. (12), we have imparted actual physical meaning to the micromechanical changes of the polymer instead of simply assuming the usual empirical approach that results in numerous extra fitting parameters bearing no actual physical meaning.

The effect of photo-oxidation on the evolution of the remaining physical variables on the intermolecular branch of Fig. 1(b) (i.e., the athermal shear yield strength s_0 and the activation energy ΔG_{a_0} in Eq. (8)) is accounted for by describing appropriate evolution functions in terms of the degradation indicator $\omega(t)$. In particular, the evolution of the athermal shear yield strength is defined as follows:

$$s(t) = s_0 \omega(t)^{-1} \tag{13}$$

where s_0 and s(t) are the athermal shear yield strengths corresponding to the unaged and aged states, respectively. Again, the inverse proportionality is justified using the same argument as the one given for the Young's modulus. Furthermore, assuming that the ratio $\frac{\Delta G_{a_0}}{s_0}$ remains

constant (Belbachir et al., 2010), the evolution of the activation energy can be expressed as follows:

$$\Delta G_a(t) = \Delta G_{a_0} \left(\frac{s(t)}{s_0} \right) \tag{14}$$

where ΔG_{a_0} is the activation energy corresponding to the initial unaged state.

Having identified the responsible mechanisms for degradation and conjectured appropriate physio-chemically based evolution functions for the material properties, in Section 4, we present the chemical characterization techniques that have been designed to measure the crystallinity and the minute mass ratio needed in the evolution (12)–(14).

4. Material characterization

In this section, information pertaining to the experimental techniques is summarized. Specific details regarding the LDPE material, the UV aging procedure for which the LDPE films were subjected to, and the experimental test measurements (*i.e.*, DSC, QCM-D, and quasi-static tensile tests) are presented. Interpretation of the experimental results is provided in Section 5.1.

4.1. Material

LDPE pellets were purchased from Sigma-Aldrich and used as received. The density of the virgin LDPE is $0.93~g/cm^2$ and the melting point is $116~^{\circ}$ C. LDPE films were prepared from thermopressing at $180~^{\circ}$ C with loading of 8 tons during 2 min. The resulting films were cooled in air from $180~^{\circ}$ C to room temperature and were subsequently thermally annealed at $110~^{\circ}$ C for 1 h. The resulting polymer films had thicknesses ranging between 30 and 80 μ m. This range of thickness was intentionally selected to allow for homogeneous oxidation and prevent diffusion-limited-oxidation (DLO) conditions (Ayoub et al., 2020; Tavares et al., 2003; Tireau et al., 2009; Hsueh et al., 2020).

4.2. UV aging

Polymer films were aged under a 250 W UV lamp at a wavelength of 254 nm (Rayonet $^{\circledR}$ RPR-100 photoreactor with a maximum UV dose of 125 kW/m²) to simulate and accelerate the LDPE photo-oxidation in air at room temperature (25 °C). It is worth mentioning that the actual temperature in the UV lamps was higher than room temperature due to electrothermal and photothermal conversions. Therefore, the working temperature of the UV lamps was 37 °C as claimed by the manufacturer. To maintain the temperature of the samples at 25 °C, the experiments were setup as presented in Fig. 3. Mirror was utilized to focus UV light on the samples. Samples were subjected to a weak cooling air flow to maintain the ambient temperature. Subsequently, the LDPE coated QCM-D sensors were aged in the UV chamber for varying aging times: 0, 24, 48, 72, and 112 h.

4.3. DSC

DSC was performed between 40 and 200 °C at a heating rate of 30 °C/min under a Nitrogen stream of 50 mL/min on a Discovery DSC2500 (TA Instruments). The DSC was calibrated using indium (melting point (m.p.) = 156.60 °C) and zinc (m.p. = 419.47 °C) standards. The crystallinity of LDPE was calculated using melting enthalpy divided by 293 J/g for 100% crystalline material. DSC characterization on films with thicknesses smaller than 1 μm is difficult due to the low sensitivity of common DSC at low sample mass. Therefore, crystallinity was measured for bulk samples (i.e., samples with thicknesses ranging between 30 and 80 μm). This range of thickness is larger than the threshold limit for which thickness effects on crystallinity measurement become significant, i.e., between 300 nm and 1000 nm (Wang et al., 2004).

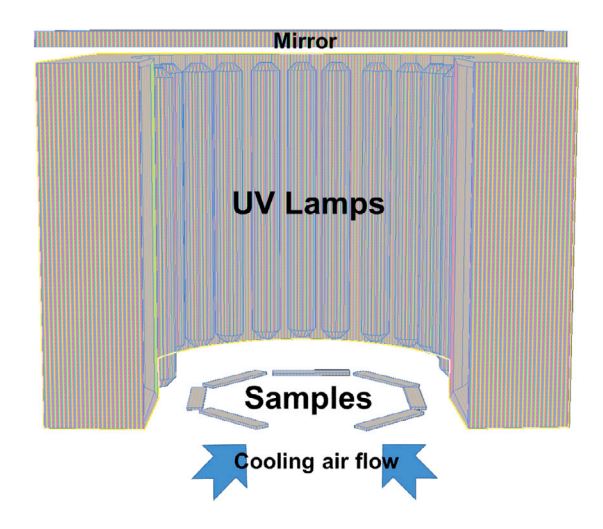


Fig. 3. Experimental setup of UV aging. Mirror was utilized to focus UV light on the samples. A roughly 1 cm gap was designed between LDPE samples and UV lamps to allow the cooling air to flow through.

4.4. QCM-D

QCM-D is a mass measurement technique that is highly surface sensitive and is mostly employed to measure the mass of layers in the nanometer thickness range. In this study, QCM-D was utilized to measure the minute mass ratio between the aged and unaged films. To investigate the effect of film thickness on the mass loss, three varying thicknesses (three parallel samples each) were prepared (i.e., 146, 158, and 200 nm) by spincoating directly on the QCM-D sensor plate. The film thicknesses were determined based on the film mass calculated from the change in frequency of the crystal upon loading and the density of the polymer. The film thickness was controlled by changing the spin speed during spincoating a xylene solution of LDPE (6 wt%). During spin-coating, the QCM-D plate and LDPE solution were heated with an IR lamp to prevent precipitation. Polymer coated plates were then thermally annealed under vacuum at the same conditions as bulk films before aging experiments and QCM-D measurements were performed. After UV aging, the LDPE coated QCM-D plates were rinsed with deionized water at room temperature to dissolve the oxidized polymer fragments. The water on the sample was carefully wiped off and samples were subsequently dried with nitrogen flow (50 mL/s). Any residual moisture was removed under vacuum at room temperature (25 °C) for 12 h. The resonance frequency of the samples was then directly measured and converted into mass using Sauerbrey equation (Sauerbrey, 1959).

4.5. Mechanical testing

Specimens of as-received and aged LDPE films were cut out into dogbones and tensile tests were conducted to determine their stress-strain response before and after aging (following ASTM-D-638 standard). To subject the specimens to quasi-static loading, samples were stretched in tensile mode up to rupture at a constant strain rate of $0.004\ s^{-1}$. At least three sample tests were performed for a given exposure time to minimize uncertainty in the observed behavior.

5. Results and discussion

5.1. Interpretation of the experimental test results

5.1.1. DSC

Fig. 4 presents the evolution of the crystallinity during photooxidation obtained based on DSC. Under the applied aging scenarios,

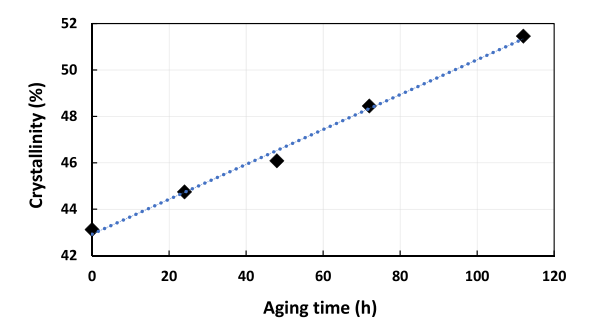


Fig. 4. Evolution of crystallinity as a function of photo-oxidation aging time obtained from the DSC test.

the degree to which the crystalline part of the material gains further chain-ordering increased linearly with aging time. In fact, after just 48 h of photo-oxidation, the crystallinity increased from an initial value of approximately 43% to 46%, totaling nearly a 7% difference. At the end of 112 h, the crystallinity reached a value of nearly 52%, which corresponds to a percent difference of about 19% from the initial value. The shift in the crystallinity in this work is similar to the work of Rodriguez et al. (2020) while the percentage difference is higher. The dissimilarity in the percent difference is because the initial crystallinity in the work of Rodriguez et al. (2020) was higher than LDPE here (i.e., 55% compared to 43%). This difference of the initial crystallinity can be attributed to the different annealing procedure. Particularly, the material which (Rodriguez et al., 2020) used was initially as crystalline as our material was after 112 h of UV aging. The difference in initial crystallinity could explain some of the discrepancies in material response behavior observed in our studies. However, it is also worth mentioning that in the work of Rodriguez et al. (2020), the aging experiments were performed with a radiance of 1.55 W/m² compared to 125 kW/m2 in our work. This means that at the end of 250 h of UV aging, their samples were subjected to a total of 1.4 MJ/m² of UV radiation compared to 50 GJ/m² in our work for a duration of 112 h. Clearly, the extent of crystallinity change is heavily dependent on the initial composition of the material as well as radiance.

The increase in crystallinity in this study contributes to a further stiffening in the material upon photo-oxidation. Whether the newly created crystallites are primary or secondary however, cannot be determined simply using Fig. 4. To this end, Fig. 5 illustrates the heating thermograms of LDPE for varying photo-oxidation aging times. It can be seen that additional endothermic shoulders appeared below the melting temperature (i.e., $\sim 105 < 125\,^{\circ}\text{C}$). However, this temperature is higher than the exposure temperature (25 °C). Therefore, these findings may indicate that the newly formed crystallites are secondary. However, as explained earlier in the manuscript, identifying the nature of these crystallites is not as important as recognizing that the crystallinity is inevitably expanded, and as a result, stiffness and ultimately embrittlement are significantly amplified.

While it is clear that the extent of crystallization increases linearly with aging time, it is expected, however, that the increase in crystallinity would reach a steady state some time later on in the aging process, in which case the stiffness would also reach a saturation state (Bhateja, 1983). Therefore, to account for this apparent linear dependency between the change in crystallinity and its effect on stiffness, a linear proportionality seems to be the right fit. Any changes in the crystallinity and its influence on stiffness (i.e., increase, constancy, or even decrease) would be appropriately captured by a linear proportionality between the initial elastic modulus and the evolution in crystallinity.

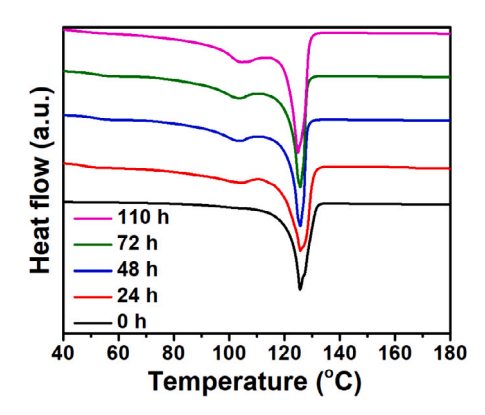


Fig. 5. DSC thermograms of LDPE after varying photo-oxidation aging times.

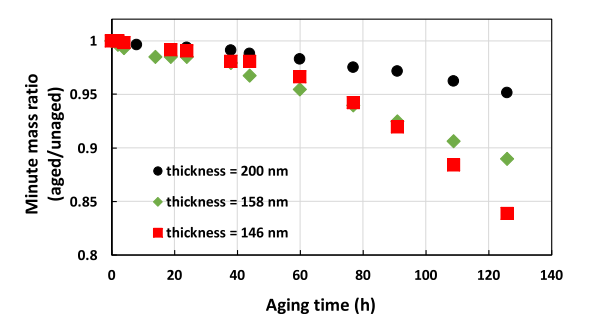


Fig. 6. Evolution of the minute mass ratio between the aged and unaged samples as a function of photo-oxidation aging time obtained from the QCM-D test. The minute mass ratio is presented for three film thicknesses; 200 nm, 158 nm, and 146 nm represented by circles, hexagons, and squares, respectively.

5.1.2. QCM-D

In this study, the hydrophobic character of LDPE means the pristine polymer is totally insoluble in water. Photoinduced oxidation and degradation of the material requires the penetration of light and oxygen into the sample. As a result, oxidation starts at the surface and evolves over time. The QCM-D technique is uniquely sensitive to mass changes in thin films where surface oxidation will affect a significant fraction of the total mass on the sensor. A gentle rinse of the film with water will remove material that has been significantly cleaved and oxidized to be soluble in water. This mass loss will cause an increase in the oscillation frequency of the crystal that can be converted to the minute mass loss through the Sauerbrey equation. This procedure should work well for any water insoluble polymer that can be spincoated onto the sensor.

Fig. 6 illustrates the evolution of the minute mass ratio with respect to aging time measured by the QCM-D for three different LDPE film thicknesses. The 200-nm-thick film experienced a nearly 5% weight loss after 120 h of UV aging. On the other hand, the two remaining thinner films experienced more weight loss under the same aging duration (i.e., up to 15% for the 146-nm-thick film). Nevertheless, given that the LDPE coated QCM-D plates were rinsed with deionized water, a 5% mass loss at 112 h of UV aging with a dose rate equal to 125 kW/m² is remarkable. Indeed, microplastics are found in exuberant amounts largely due to plastic-fragmentation caused by the exposure of plastics to environmental perturbations such as UV radiation.

5.1.3. Mechanical testing

Tensile stress–strain curves for LDPE were obtained for the aging times considered in this work (i.e., 0, 48, 74, 98, and 112 h). At least three replicates were tested for each aging time. The averages amongst each group of replicates were taken and the result were plotted in Fig. 7. The true stress–strain measures were used to describe the deformation behavior of the material. The uniaxial true strain, $\epsilon_{\rm true}$,

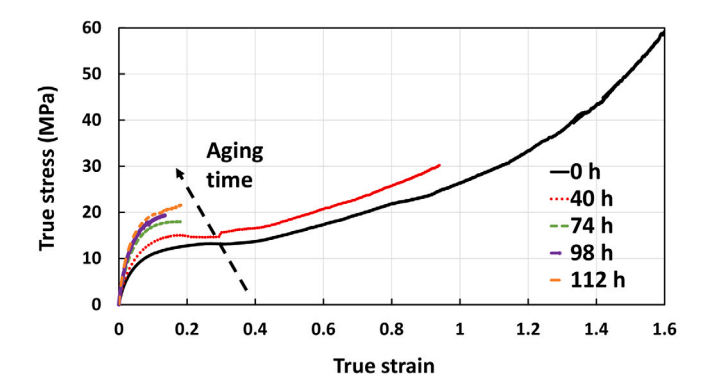


Fig. 7. Average engineering stress-strain curves from each group of at least three replicates corresponding to different photo-oxidation aging times (i.e., 0, 40, 74, 98, and 112 h).

was obtained as $\epsilon_{\rm true} = \ln(\epsilon_{\rm eng} + 1)$ where $\epsilon_{\rm eng}$ is the uniaxial engineering strain measured by the Instron machine; whereas the uniaxial true stress, $\sigma_{\rm true}$, was obtained as $\sigma_{\rm true} = \sigma_{\rm eng} \times (\epsilon_{\rm eng} + 1)$ where $\sigma_{\rm eng}$ is the uniaxial tensile engineering stress measured by the Instron. Note that since fracture was not implemented in our framework, the obtained stress–strain curves shown in Fig. 7 have been simply interrupted at the experimental values for the corresponding strain to fracture.

It can be seen that both the initial stiffness and the yield stress increased by increasing aging time. On the other hand, the films showed a substantial reduction in ductility. The increase in the initial stiffness and yield stress are indicative of chemi-crystallization and chain crosslinking. The loss of ductility is indicative of a reduction in the molecular weight. The observed effects of photo-oxidation on the mechanical performance of LDPE (i.e., increase in initial stiffness and yield stress and decrease in ductility) are expected and supported by the characterizations of DSC and QCM-D. On the one hand, the expansion of the crystalline domain at the expense of its amorphous counterpart after long aging times explains the enhanced initial stiffness and yield stress. On the other hand, the minute mass loss determined by the QCM-D indicates LDPE degradation during photo-oxidation which reduces chain integrity and compromises the mechanical response, causing a substantial decrease in material ductility over exposure time. Here, it is worth mentioning that although the weight loss in bulk polymer films may not be comparable with that of thin films under the same aging conditions, the loss of LDPE chain integrity after photo-oxidation is expected be comparable for both thin and bulk polymer films due to the good UV light transmittance in polyethylene at thicknesses lower than 80 µm. Therefore, other than the crystallinity change determined by DSC, the reduced ductility after photo-oxidation is also explained by the mass loss monitored by QCM-D.

5.2. Prediction capability of the proposed constitutive framework

In this section, prediction capability of the proposed constitutive framework is discussed. The constitutive framework was numerically implemented into a Matlab code for the case of uniaxial tensile loading.

We reiterate that contrary to the existing works (e.g., Rodriguez et al., 2020; Ayoub et al., 2020; Belbachir et al., 2010), we do not fit the constitutive equations to the *aged* experimental stress–strain curves. Instead, we propose evolution functions for the relevant material properties in terms of the crystallinity and mass loss as they evolve during photo-oxidation. As such, the evolution functions do not contain any extra fitting parameters that lack physical meaning; rather, they are simply expressed in terms of the evolving physio-chemical properties and the corresponding values at the *unaged* configuration (i.e., E_0 , s_0 , and ΔG_{a_0}). The material properties associated with the unaged configuration can be obtained by fitting the unaged specimen's stress–strain response, which is the only fitting that we conduct. Once the

Table 1
Material properties for the unaged LDPE specimen.

Branch contribution	Parameters	Equation	Values
Intermolecular resistance	Elastic modulus (MPa), E_0	(6)	596
	Poisson's ratio, v	(6)	0.49
	Pre-exponential factor (s^{-1}), $\dot{\gamma}_0$	(8)	1.75×10^{6}
	Athermal shear yield strength (MPa), s_0	(8)	155
	Activation energy (J), ΔG_{a_0}	(8)	8.5×10^{-17}
Network resistance	Rubbery modulus (MPa), μ_0	(9)	2.3
	Number of Kuhn monomers, N_{k_0}	(9)	100
	Relaxation parameter (MPa^{-1}) , C	(11)	8×10^{-8}

unaged material properties are determined, their evolution according to the proposed evolution functions (i.e., Eqs. (12)–(14)) can be readily acquired for any aging time. Fig. 8 illustrates a procedural flowchart for the identification of the material properties and the prediction and validation of the proposed constitutive framework.

To begin, the unaged tensile test was used to determine the material properties of the unaged film involved in the constitutive framework (i.e., E_0 , s_0 , ΔG_{a_0} , μ_0 , and N_{k_0}). Specifically, the elastic modulus E_0 and the rubber modulus μ_0 were determined as the slope of the lowstrain and the large-strain regions of the tensile stress-strain curve, respectively. Additionally, the athermal shear yield strength s_0 , the activation energy ΔG_{a_0} , and the number of Kuhn monomers N_{k_0} were determined by fitting the unaged stress-strain curve to the numerical response. An alternative method to obtain s_0 and ΔG_{a_0} is through conducting tensile tests at varying strain rates and using (8) to backcalculate the values of the two properties. Table 1 summarizes the obtained unaged material properties and Fig. 9 illustrates the comparison between the unaged numerical and experimental true stress-strain responses. Once the unaged material properties were determined, their evolution according to the proposed evolution functions (i.e., Eqs. (12)-(14)) for any aging time could be readily acquired. Therefore, the predicted responses for the aged configurations are based solely on the proposed physics-based and chemistry-motivated evolution functions for the key macromechanical model parameters. No additional fitting variables are required for our predictions.

Fig. 10 demonstrates the comparison between the experimental tensile test and the developed constitutive framework for photo-oxidatively aged LDPE under varying exposure times. Particularly, Fig. 10(a) summarizes the comparison results from all of the considered aging times, while Figs. 10(b)-10(e) focus on the response predictions at each aging time separately to better appreciate the accuracy of predictions. A very good prediction could be obtained for all aging times. Both the initial modulus and the yield stress accurately matched with the experimental results for the varying aging times considered in this study.

5.3. Discussion

Physio-chemically-motivated evolution functions based on LDPE film minute mass loss and crystallinity changes are important for accurate prediction of photo-oxidation effects on the mechanical response of LDPE. Obtaining the minute mass loss evolution functions is challenging primarily due to the minor weight loss and negligible mass change for thick polymer films. Therefore, to accurately measure the mass loss during aging, the use of thin films is inevitable. However, when it comes to thin films, the thickness effect on the film behavior is considerable. For instance, the film thickness has an observable effect on the glass transition temperature of polymer when it is around 100 nm due to the increased surface effect of thin films (Peter et al., 2006). Therefore, to consider the minor mass loss for thick films and avoid spurious thickness effects for thin films, LDPE films with thickness less than 1 µm but greater than 100 nm can be used to amplify the mass loss under the aging conditions and accurately measure the change of mass. Indeed, an increase in the film thickness in the QCM-D

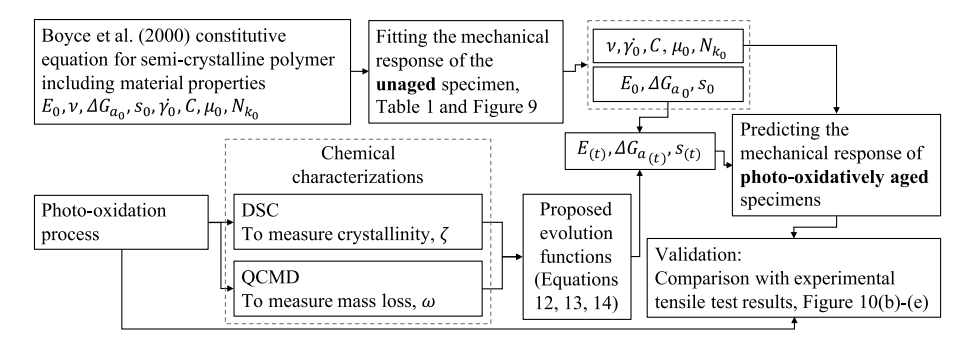


Fig. 8. Procedural flowchart for the identification of the material properties and the prediction and validation of the constitutive framework.

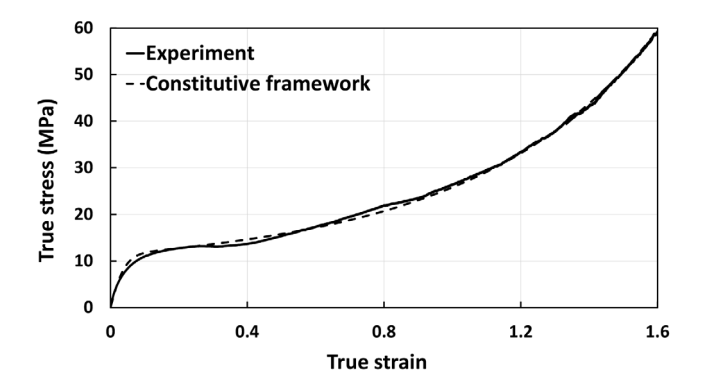


Fig. 9. True stress-strain curve of unaged LDPE representing the experiment versus numerical response based on the constitutive framework.

measurement may further improve the accuracy and reliability of result predictions; nonetheless, based on the mass loss evolution of films with thickness equal to 200 nm, the proposed constitutive framework already can predict the mechanical responses of photo-oxidatively aged semi-crystalline LDPE very well as it can be seen in Fig. 10.

In addition to the minute mass loss, crystallinity behavior also merits careful attention. In particular, the initial crystallinity determined in this work was relatively lower than the one reported by Rodriguez et al. (2020). The difference in the measured initial crystallinity may have had a significant contribution to the variations observed in the mechanical responses of unaged and aged samples between our study and the study by Rodriguez et al. (2020). Indeed, after 112 h of UV radiation with an intensity of 125 kW/m², our material was just as crystalline as the material used in Rodriguez et al. (2020) initially was (i.e., before any UV exposure). Additionally, investigation of Scanning Electron Microscopy (SEM) images on aged samples (which are not included here for brevity) showed that the material did not exhibit any observable defects or pore generation of sizes greater than 10 nm either on the surface or on the cross-sections that would cause the softening in stiffness or yielding that was observed in Rodriguez et al. (2020). The differences in the microstructural observations between our two studies may have had to do with the initial material composition; particularly, the difference in the initial crystallinity discussed herein. Therefore, comparison between both of these works should be approached with care to make meaningful conclusions regarding crystallinity change effects on the evolution of LDPE material properties.

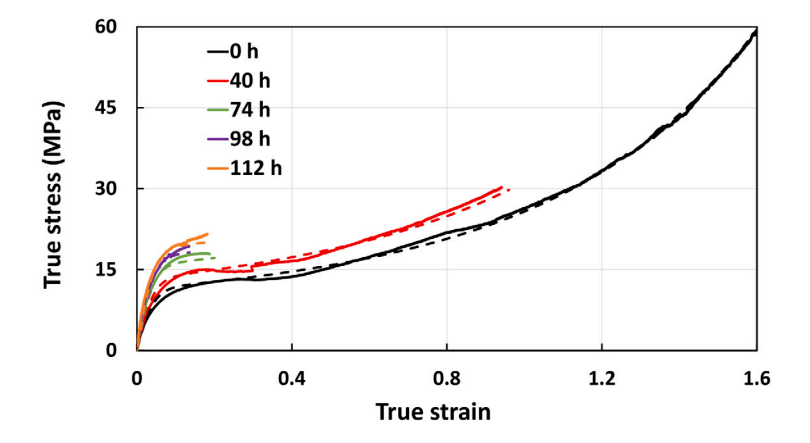
The ability of the developed constitutive framework to accurately predict the mechanical test results of aged LDPE independently of any mechanical tests on the aged configurations constitutes the important contribution of the proposed framework. Indeed, many if not all of the existing works use several mechanical tests to fit the constitutive law to the aged responses and obtain fitting parameters that carry no physical

meaning within the overall material behavior (Ayoub et al., 2020; Lamnii et al., 2021; Belbachir et al., 2010). Doing so renders the constitutive approach essentially a fitting algorithm with numerous fitting parameters that only apply to the specific problem for which calibration was performed. In contrast, developing a general, self-contained, and robust framework that is physics- and chemistry-based and is comprehensive in its prediction capability is more reliable. Nevertheless, it serves to mention that although the evolution functions were not explicitly developed based on thermodynamic laws, the ability to express them in a self-contained manner that is chemistry-motivated provides a great contribution to the existing predictive efforts. Indeed, by recognizing that changes in the stiffness, yield strength, and activation energy can be directly linked to crystallinity and mass loss changes during photo-oxidation, we have shown that it is possible to develop robust micromechanically-motivated expressions for their evolution response. Therefore, the developed physio-chemically-motivated framework is unique and unprecedented.

6. Concluding remarks

We developed a purely physio-chemically-based constitutive framework to predict the mechanical performance of semi-crystalline LDPE in response to photo-oxidative aging. In contrast to all modeling efforts in the literature, we based the evolution of the macromechanical properties in response to photo-oxidation on the chemically verified processes responsible for material degradation. In doing so, we eliminated the need to employ extra fitting parameters which carry no physical meaning. The framework was based on modifying the constitutive equations of Boyce et al. (2000) to incorporate the effects of crystallinity evolution and minute mass ratio change in modifying the elasto-viscoplastic material properties. The crystallinity change was measured with DSC whereas the minute mass loss was measured with QCM-D. The use of QCM-D as a characterization technique for photo-oxidation investigation was validated through comparison between numerical and experimental tensile test results. Particularly, we showed that the minute mass ratio can be directly related to polymer stiffening and increase in yield stress and conjectured appropriate evolution functions for the material properties probing polymer response to chemical changes. These chemical characterizations (i.e., DSC and OCM-D) determined the changes in the physio-chemical structure of the material and bridged the gap between molecular network evolution and its effect on the overall macroscopic mechanical changes. The developed constitutive framework could predict the mechanical responses of photo-oxidatively aged LDPE independently of mechanical tests on aged specimens with high accuracy. It thus provides a oneto-one mapping between chemistry-based quantities (i.e., crystallinity and minute mass ratio) and physics-based macroscopic variables (i.e., elasto-viscoplastic mechanical properties of the material).

A possible future investigation is to implement the developed threedimensional constitutive framework into a finite element software



(a) All aging times

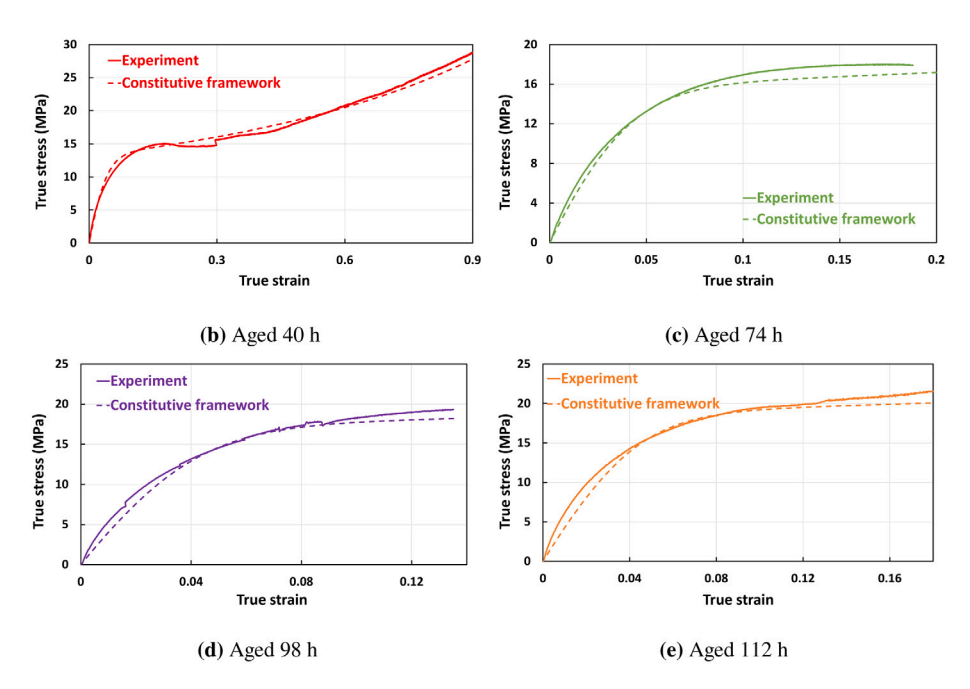


Fig. 10. Constitutive framework prediction versus experimental results for the varying aging times considered in this work.

that allows for various additional considerations (e.g., more complex load states, coupled chemo-mechanical diffusion problem, etc.). This can be realized through the incorporation of kinetics equations based on the chemical characterizations presented in this work (i.e., crystallinity change and evolution of mass loss) coupled with a diffusion-deformation problem. Another possible future study is to incorporate damage into the developed constitutive framework to capture photo-oxidation-induced failure of aged polymers. Consideration of such important developments is particularly essential in ensuring durable polymer design and active environment protection and is the topic of future work by the authors.

Declaration of competing interest

The authors declare that they have no known competing financial interests or personal relationships that could have appeared to influence the work reported in this paper.

Acknowledgment

The authors gratefully acknowledge the support from the National Science Foundation, USA under the award number CMMI-1914565.

Appendix

The determinant of the total deformation gradient \mathbf{F} , det \mathbf{F} , can be multiplicatively decomposed into elastic and plastic components as det $\mathbf{F} = J^eJ^p > 1$, in which we define $J^e = \det \mathbf{F}^e$ and $J^p = \det \mathbf{F}^p$. Assuming that plastic flow is volume preserving (i.e., incompressible), we write $J^p = \det \mathbf{F}^p = 1$. Note that the decomposition used in Eqs. (3) indicates that there exists an intermediate configuration (i.e., a relaxed configuration) between the undeformed and the current configurations. The relaxed configuration is assumed to be obtained from the current configuration by unloading through the inverse of the elastic part of the deformation gradients.

Additionally, we can use the polar decomposition of the deformation gradients Eqs. (3) and write (Gurtin and Anand, 2005):

$$\mathbf{F}_{I} = \mathbf{V}_{I}^{e} \mathbf{R}_{I}^{e} \mathbf{V}_{I}^{p} \mathbf{R}_{I}^{p} \tag{15}$$

$$\mathbf{F}_N = \mathbf{V}_N^e \mathbf{R}_N^e \mathbf{V}_N^p \mathbf{R}_N^p \tag{16}$$

where V and R refer to the stretch (symmetric) and rotation (orthogonal) parts of the corresponding deformation gradient, respectively.

The velocity gradients $\mathbf{L}_I = \dot{\mathbf{F}}_I \mathbf{F}_I^{-1}$ for branch I and $\mathbf{L}_N = \dot{\mathbf{F}}_N \mathbf{F}_N^{-1}$ for branch N can be computed as follows:

$$\mathbf{L}_{I} = \dot{\mathbf{F}}_{I} \mathbf{F}_{I}^{-1} = \dot{\mathbf{F}}_{I}^{e} \mathbf{F}_{I}^{e-1} + \mathbf{F}_{I}^{e} \dot{\mathbf{F}}_{I}^{p} \mathbf{F}_{I}^{p-1} \mathbf{F}_{I}^{e-1} = \mathbf{L}_{I}^{e} + \mathbf{L}_{I}^{p}$$
(17)

$$\mathbf{L}_{N} = \dot{\mathbf{F}}_{N} \mathbf{F}_{N}^{-1} = \dot{\mathbf{F}}_{N}^{e} \mathbf{F}_{N}^{e^{-1}} + \mathbf{F}_{N}^{e} \dot{\mathbf{F}}_{N}^{p} \mathbf{F}_{N}^{p^{-1}} \mathbf{F}_{N}^{e^{-1}} = \mathbf{L}_{N}^{e} + \mathbf{L}_{N}^{p}$$
(18)

The plastic components of the velocity gradients $\mathbf{L}_I^p = \mathbf{F}_I^e \dot{\mathbf{F}}_I^p \mathbf{F}_I^{p-1} \mathbf{F}_I^{e-1}$ and $\mathbf{L}_N^p = \mathbf{F}_N^e \dot{\mathbf{F}}_N^p \mathbf{F}_N^{p-1} \mathbf{F}_N^{e-1}$ can also further be decomposed into their symmetric and skew parts as follows:

$$\mathbf{L}_{I}^{p} = \mathbf{D}_{I}^{p} + \mathbf{W}_{I}^{p} \tag{19}$$

$$\mathbf{L}_{N}^{p} = \mathbf{D}_{N}^{p} + \mathbf{W}_{N}^{p} \tag{20}$$

where \mathbf{D}_{I}^{p} and \mathbf{D}_{N}^{p} are the rates of inelastic deformation, and \mathbf{W}_{I}^{p} and \mathbf{W}_{N}^{p} are the inelastic spins which are assumed, without loss of generality, to be equal to zero (*i.e.*, irrotational).

References

- Abdelaziz, M.N., Ayoub, G., Colin, X., Benhassine, M., Mouwakeh, M., 2019. New developments in fracture of rubbers: Predictive tools and influence of thermal aging. Int. J. Solids Struct. 165, 127–136.
- Abdul-Hameed, H., Messager, T., Zaïri, F., Naït-Abdelaziz, M., 2014. Large-strain viscoelastic-viscoplastic constitutive modeling of semi-crystalline polymers and model identification by deterministic/evolutionary approach. Comput. Mater. Sci. 90, 241–252.
- Ahzi, S., Makradi, A., Gregory, R., Edie, D., 2003. Modeling of deformation behavior and strain-induced crystallization in poly (ethylene terephthalate) above the glass transition temperature. Mech. Mater. 35 (12), 1139–1148.
- Anand, L., Gurtin, M.E., 2003. A theory of amorphous solids undergoing large deformations, with application to polymeric glasses. Int. J. Solids Struct. 40 (6), 1465–1487.
- Arruda, E.M., Boyce, M.C., 1993. A three-dimensional constitutive model for the large stretch behavior of rubber elastic materials. J. Mech. Phys. Solids 41 (2), 389–412.
- Arruda, E.M., Boyce, M.C., Jayachandran, R., 1995. Effects of strain rate, temperature and thermomechanical coupling on the finite strain deformation of glassy polymers. Mech. Mater. 19 (2–3), 193–212.
- Ayoub, G., Rodriguez, A., Mansoor, B., Colin, X., 2020. Modeling the visco-hyperelastic-viscoplastic behavior of photodegraded semi-crystalline low-density polyethylene films. Int. J. Solids Struct. 204, 187–198.
- Ayoub, G., Zaïri, F., Naït-Abdelaziz, M., Gloaguen, J.M., 2010. Modelling large deformation behaviour under loading-unloading of semicrystalline polymers: application to a high density polyethylene. Int. J. Plast. 26 (3), 329–347.
- Bardenhagen, S.G., Stout, M.G., Gray, G.T., 1997. Three-dimensional, finite deformation, viscoplastic constitutive models for polymeric materials. Mech. Mater. 25 (4), 235–253.
- Belbachir, S., Zaïri, F., Ayoub, G., Maschke, U., Naït-Abdelaziz, M., Gloaguen, J.M., Benguediab, M., Lefebvre, J.M., 2010. Modelling of photodegradation effect on elastic-viscoplastic behaviour of amorphous polylactic acid films. J. Mech. Phys. Solids 58 (2), 241–255.
- Bergmann, M., Mützel, S., Primpke, S., Tekman, M.B., Trachsel, J., Gerdts, G., 2019.
 White and wonderful? Microplastics prevail in snow from the alps to the arctic.
 Sci. Adv. 5 (8), eaax1157.
- Bhateja, S., 1983. Radiation-induced crystallinity changes in linear polyethylene: Influence of aging. Int. J. Plast. 28 (2), 861–872.
- Boyce, M.C., Parks, D.M., Argon, A.S., 1988. Large inelastic deformation of glassy polymers. Part I: rate dependent constitutive model. Mech. Mater. 7 (1), 15–33.
- Boyce, M., Socrate, S., Llana, P., 2000. Constitutive model for the finite deformation stress-strain behavior of poly (ethylene terephthalate) above the glass transition. Polymer 41 (6), 2183–2201.
- Brandon, J., Goldstein, M., Ohman, M.D., 2016. Long-term aging and degradation of microplastic particles: comparing in situ oceanic and experimental weathering patterns. Mar. Pollut. Bull. 110 (1), 299–308.
- Breche, Q., Chagnon, G., Machado, G., Girard, E., Nottelet, B., Garric, X., Favier, D., 2016a. Mechanical behaviour's evolution of a PLA-b-PEG-b-PLA triblock copolymer during hydrolytic degradation. J. Mech. Behav. Biomed. Mater. 60, 288–300.
- Breche, Q., Chagnon, G., Machado, G., Nottelet, B., Garric, X., Girard, E., Favier, D.,
 2016b. A non-linear viscoelastic model to describe the mechanical behavior's
 evolution of biodegradable polymers during hydrolytic degradation. Polym. Degrad.
- Carrasco, F., Pagès, P., Pascual, S., Colom, X., 2001. Artificial aging of high-density polyethylene by ultraviolet irradiation. Eur. Polym. J. 37 (7), 1457–1464.
- Celina, M.C., 2013. Review of polymer oxidation and its relationship with materials performance and lifetime prediction. Polym. Degrad. Stab. 98 (12), 2419–2429.

- Cohen, A., 1991. A Padé approximant to the inverse Langevin function. Rheol. Acta 30 (3), 270–273.
- Cundiff, K., Madi, Y., Benzerga, A., 2020. Photo-oxidation of semicrystalline polymers: Damage nucleation versus growth. Polymer 188, 122090.
- Da Costa, J.P., Nunes, A.R., Santos, P.S., Girao, A.V., Duarte, A.C., Rocha-Santos, T., 2018. Degradation of polyethylene microplastics in seawater: Insights into the environmental degradation of polymers. J. Environ. Sci. Health A 53 (9), 866–875.
- Dupaix, R.B., Krishnan, D., 2006. A constitutive model for strain-induced crystallization in poly (ethylene terephthalate)(PET) during finite strain load-hold simulations. J. Eng. Mater. Technol. 128 (1), 28–33.
- Fayolle, B., Richaud, E., Colin, X., Verdu, J., 2008. Degradation-induced embrittlement in semi-crystalline polymers having their amorphous phase in rubbery state. J. Mater. Sci. 43 (22), 6999–7012.
- Guo, X., Wang, J., 2019. The chemical behaviors of microplastics in marine environment: A review. Mar. Pollut. Bull. 142, 1–14.
- Gurtin, M.E., Anand, L., 2005. The decomposition f=fefp, material symmetry, and plastic irrotationality for solids that are isotropic-viscoplastic or amorphous. Int. J. Plast. 21 (9), 1686–1719.
- Han, X., Pan, J., 2009. A model for simultaneous crystallisation and biodegradation of biodegradable polymers. Biomaterials 30 (3), 423–430.
- Hedir, A., Moudoud, M., Lamrous, O., Rondot, S., Jbara, O., Dony, P., 2020. Ultraviolet radiation aging impact on physicochemical properties of crosslinked polyethylene cable insulation. J. Appl. Polym. Sci. 137 (16), 48575.
- Hsu, Y.-C., Weir, M.P., Truss, R.W., Garvey, C.J., Nicholson, T.M., Halley, P.J., 2012. A fundamental study on photo-oxidative degradation of linear low density polyethylene films at embrittlement. Polymer 53 (12), 2385–2393.
- Hsueh, H.-C., Kim, J.H., Orski, S., Fairbrother, A., Jacobs, D., Perry, L., Hunston, D., White, C., Sung, L., 2020. Micro and macroscopic mechanical behaviors of highdensity polyethylene under UV irradiation and temperature. Polym. Degrad. Stab. 174, 109098.
- Johlitz, M., Diercks, N., Lion, A., 2014. Thermo-oxidative ageing of elastomers: A modelling approach based on a finite strain theory. Int. J. Plast. 63, 138–151.
- Julienne, F., Lagarde, F., Delorme, N., 2019a. Influence of the crystalline structure on the fragmentation of weathered polyolefines. Polym. Degrad. Stab. 170, 109012.
- Julienne, F., Lagarde, F., Delorme, N., 2019b. Influence of the crystalline structure on the fragmentation of weathered polyolefines. Polym. Degrad. Stab. 170, 109012.
- Kershaw, P., Rochman, C., 2015. Sources, fate and effects of microplastics in the marine environment: part 2 of a global assessment. Reports And Studies-IMO/FAO/Unesco-IOC/WMO/IAEA/UN/UNEP Joint Group Of Experts On The Scientific Aspects Of Marine Environmental Protection (GESAMP) Eng No. 93, IMO/FAO/UNESCO-IOC/ÚNIDO/WMO/IAEA/UN/INFE/JUNDP
- Lamnii, H., Abdelaziz, M.N., Ayoub, G., Colin, X., Maschke, U., 2021. Experimental investigation and modeling attempt on the effects of ultraviolet aging on the fatigue behavior of an LDPE semi-crystalline polymer. Int. J. Fatigue 142, 105952.
- Lee, E.H., 1969. Elastic-plastic deformation at finite strains. J. Appl. Mech. 36 (1), 1–6.
 Makradi, A., Ahzi, S., Gregory, R., Edie, D., 2005. A two-phase self-consistent model for the deformation and phase transformation behavior of polymers above the glass transition temperature: application to PET. Int. J. Plast. 21 (4), 741–758.
- Mohammadi, H., Morovati, V., Korayem, A.-E., Poshtan, E., Dargazany, R., 2021. Constitutive modeling of elastomers during photo- and thermo-oxidative aging. Polym. Degrad. Stab. 191, 109663.
- Peter, S., Meyer, H., Baschnagel, J., 2006. Thickness-dependent reduction of the glass-transition temperature in thin polymer films with a free surface. J. Polym. Sci. B 44 (20), 2951–2967.
- Rabek, J.F., 1994. Polymer Photodegradation: Mechanisms And Experimental Methods. Springer Science & Business Media.
- Rabello, M., White, J., 1997. Crystallization and melting behaviour of photodegraded polypropylene—I. Chemi-crystallization. Polymer 38 (26), 6379–6387.
- Ranjan, V.P., Goel, S., 2019. Degradation of low-density polyethylene film exposed to UV radiation in four environments. J. Hazard. Toxic Radioact. Waste 23 (4), 04019015.
- Rodriguez, A., Mansoor, B., Ayoub, G., Colin, X., Benzerga, A., 2020. Effect of UV-aging on the mechanical and fracture behavior of low density polyethylene. Polym. Degrad. Stab. 180, 109185.
- Sauerbrey, G., 1959. Verwendung von Schwingquarzen zur Wägung dünner Schichten und zur Mikrowägung. Z. Phys. 155 (2), 206–222.
- Shakiba, M., Darabi, M.K., Al-Rub, R.K.A., 2016. A thermodynamic framework for constitutive modeling of coupled moisture-mechanical induced damage in partially saturated viscous porous media. Mech. Mater. 96, 53–75.
- Shakiba, M., Najmeddine, A., 2021. Physics-based constitutive equation for thermochemical aging in elastomers based on crosslink density evolution. arXiv preprint arXiv:2104.09001.
- Shlyapintokh, V.Y., 1983. Synergistic phenomena in polymer photostabilization. Pure Appl. Chem. 55 (10), 1661–1668.
- Soares, J.S., Moore, Jr., J.E., Rajagopal, K.R., 2008. Constitutive framework for biodegradable polymers with applications to biodegradable stents. Asaio J. 54 (3), 295–301.
- Soares, J.S., Rajagopal, K.R., Moore, J.E., 2010. Deformation-induced hydrolysis of a degradable polymeric cylindrical annulus. Biomech. Model. Mechanobiol. 9 (2), 177–186

- Suresh, B., Maruthamuthu, S., Kannan, M., Chandramohan, A., 2011. Mechanical and surface properties of low-density polyethylene film modified by photo-oxidation. Polym. J. 43 (4), 398–406.
- Tavares, A.C., Gulmine, J.V., Lepienski, C.M., Akcelrud, L., 2003. The effect of accelerated aging on the surface mechanical properties of polyethylene. Polym. Degrad. Stab. 81 (2), 367–373.
- Tervoort, T., Smit, R., Brekelmans, W., Govaert, L., 1997. A constitutive equation for the elasto-viscoplastic deformation of glassy polymers. Mech. Time-Dependent Mater. 1 (3), 269–291.
- Tireau, J., Van Schoors, L., Benzarti, K., Colin, X., 2009. Environmental ageing of carbon black-filled polyethylene sheaths employed in civil engineering. J. Nanostruct. Polym. Nanocompos 5, 94–100.
- Vieira, A.C., Guedes, R.M., Tita, V., 2014. Constitutive modeling of biodegradable polymers: Hydrolytic degradation and time-dependent behavior. Int. J. Solids Struct. 51 (5), 1164–1174.

- Vieira, A., Marques, A., Guedes, R., Tita, V., 2011. Material model proposal for biodegradable materials. Procedia Eng. 10, 1597–1602.
- Wang, Y., Ge, S., Rafailovich, M., Sokolov, J., Zou, Y., Ade, H., Lüning, J., Lustiger, A., Maron, G., 2004. Crystallization in the thin and ultrathin films of poly (ethylene- vinyl acetate) and linear low-density polyethylene. Macromolecules 37 (9), 3319–3327.
- Wang, Y., Han, X., Pan, J., Sinka, C., 2010. An entropy spring model for the Young's modulus change of biodegradable polymers during biodegradation. J. Mech. Behav. Biomed. Mater. 3 (1), 14–21.
- Yousif, E., Haddad, R., 2013. Photodegradation and photostabilization of polymers, especially polystyrene. SpringerPlus 2 (1), 1–32.
- Zhao, B., Zikry, M., 2017. Oxidation-induced failure in semi-crystalline organic thin films. Int. J. Solids Struct. 109, 72–83.